Applied Catalysis B: Environmental 219 (2017) 603–610

Contents lists available at ScienceDirect

Applied Catalysis B: Environmental

journal homepage: www.elsevier.com/locate/apcatb

Pentanuclear Yb(III) cluster-based metal-organic frameworks as heterogeneous catalysts for CO_2 conversion

Na Wei [a], Yue Zhang [a], Lin Liu [a], Zheng-Bo Han [a,*], Da-Qiang Yuan [b,*]

[a] College of Chemistry, Liaoning University, Shenyang 110036, PR China
[b] State Key Laboratory of Structural Chemistry, Fujian Institute of Research on the Structure of Matter, Chinese Academy of Sciences, Fuzhou 350002, PR China

ARTICLE INFO

Article history:
Received 25 February 2017
Received in revised form 26 July 2017
Accepted 28 July 2017
Available online 4 August 2017

Keywords:
Metal-organic framework
Yb_5 cluster
Polyhedral cage
Heterogeneous catalyst
CO_2 conversion

ABSTRACT

Two porous metal-organic frameworks (MOFs) incorporating pentanuclear Yb(III) clusters and pyridyl-supported tetracarboxylates or pyridyl carboxylic acid-supported tetracarboxylates, **Yb-DDPY** and **Yb-DDIA**, are presented, in which the pentanuclear Yb(III) cluster shows uncommon trigonal bipyramidal geometry. Furthermore, the pentanuclear Yb(III) clusters are extended by tetracarboxylates to form a 3D porous framework with uniform $M_{12}L_8$-cages constructed by 12 pentanuclear Yb(III) clusters and 8 tetracarboxylates with the size of *ca.* 20 Å × 17 Å. Their highly CO_2 uptake capacity and the existence of Lewis acidic sites make these MOFs promising catalysts for the chemical conversion of CO_2. These MOFs demonstrate good catalytic activities and recyclability in the cycloaddition of CO_2 and epoxides at 60 °C under 1.0 MPa pressure or at room temperature and atmospheric pressure. In addition, the synergistic effect of the Brønsted acidic –COOH groups and the Lewis acidic Yb(III) sites makes **Yb-DDIA** exhibit higher catalytic activity towards the cycloaddition of CO_2 and epoxides.

1. Introduction

Metal–organic frameworks (MOFs) as a special class of solid state materials continue to attract remarkable attentions [1] contributing to their structural diversity and tunable functionality [2]. Due to the devisable characteristic of MOFs, their structural diversity could be realized by adopting structural modules, such as organic linkers and metal/metal cluster centers with various dimensions and shapes as building units [3]. Introduction of the building units with different inherent functional moieties during the MOFs assembly or decoration of building units through post-synthetic modification are both ideal approaches to endow the MOFs potential applications [4,5].

Considered to the intriguing structural characteristics and chemical properties of multinuclear lanthanide (Ln) clusters [6–8], MOFs constructed by Ln clusters moieties have become a powerful candidate of the functional materials explored by scientists. Compared with widely studied discrete pentanuclear Ln clusters, the Ln_5 cluster-based MOFs have been rarely reported [9,10]. The existing Ln_5 clusters exhibit several classical configurations, such as square pyramidal geometry [11], vertex-fused triangular geometry [12] and trigonal bipyramidal geometry [13]. The last one is particularly rare because its forming process is complicated, which is influenced by the effect of electrostatic repulsion or ligand field stabilization energy [14]. In this work, two trigonal bipyramidal Yb_5 clusters-based MOFs, $[Yb_5(\mu_3\text{-}OH)_6(L)_2(H_2O)_6](NO_3)\cdot(solv)_x$ (L = DDPY (**Yb-DDPY**) and DDIA (**Yb-DDIA**)), were synthesized by using two different pyridyl-supported tetracarboxylates (H_4DDPY and H_4DDIA, H_4DDPY = 2,5-di(3,5-dicarboxylphenyl)pyridine and H_4DDIA = 2,5-di(3,5-dicarboxylphenyl)isonicotinic acid, Figs. S1 and S2). Both of them contain polyhedral $M_{12}L_8$-cages assembled by 12 Yb_5 clusters and 8 ligands. To the best of our knowledge, the Ln_5 cluster-based MOFs with unique polyhedral cages have not been documented. The constructed MOFs implement manifold functionalities including remarkable CO_2 adsorption and recyclable heterogeneous catalysis towards the cycloaddition of CO_2 and epoxides. Remarkably, **Yb-DDIA** shows higher catalytic activity towards the cycloaddition of CO_2 and epoxides because of the synergistic effect of the Brønsted acidic –COOH groups and the Lewis acidic Yb(III) sites.

2. Experimental

2.1. Materials and methods

All chemicals for synthesis were commercially available reagents of analytical grade and were used without further purifi-

* Corresponding authors.
E-mail addresses: ceshzb@lnu.edu.cn, zhengbo_han@163.com (Z.-B. Han), ydq@fjirsm.ac.cn (D.-Q. Yuan).

http://dx.doi.org/10.1016/j.apcatb.2017.07.085
0926-3373/

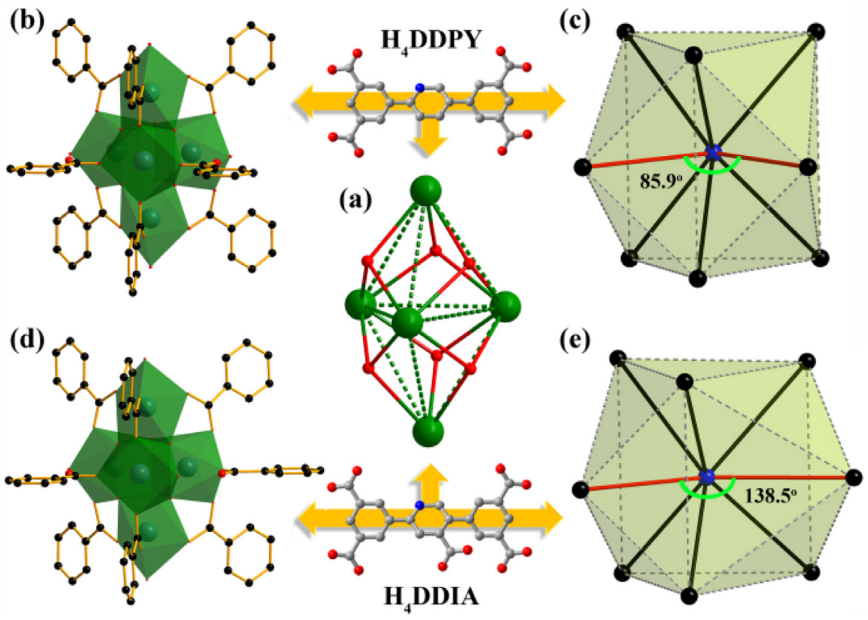

Fig. 1. (a) Pentanuclear $[Yb_5(\mu_3\text{-}OH)_6]^{9+}$ SBU with uncommon trigonal bipyramidal geometry. Linker orientation and local environment of Yb_5 clusters in Yb-DDPY (b-c) and Yb-DDIA (d-e).

cation. The C, H, and N microanalyses were carried out with Perkin-Elmer 240 elemental analyzer. Gas adsorption-desorption experiments were carried out on a Micrometritics ASAP 2020 system at various temperatures. The FT-IR spectra were recorded from KBr pellets in the 4000–400 cm^{-1} range on a Nicolet 5DX spectrometer. Thermogravimetric analyses (TGA) were taken on a Perkin-Elmer Pyrisl (25–700 °C, 5 °C min^{-1}, flowing N_2 (g)). X-ray powder diffraction was recorded with a Bruker AXS D8 advanced automated diffractometer with Cu-Kα radiation. The products of catalysis reaction are monitored by Gas chromatography with a SP-2100A Gas chromatograph. Pyridine adsorption fourier-transform infrared (Py-IR) spectra were collected on a PE FT-IR Frontier spectrometer. ^1H NMR spectra were recorded on a Varian–300 MHz NMR spectrometer.

2.2. Preparation of $[Yb_5(\mu_3\text{-}OH)_6(DDPY)_2(H_2O)_6](NO_3)\cdot(solv)_x$ (Yb-DDPY)

A solution of H_4DDPY (5 mg, 0.012 mmol), $Yb(NO_3)_3\cdot 5H_2O$ (15 mg, 0.033 mmol), DMF (2 mL) and H_2O (1 mL) was placed in a screw-capped vial and subsequently heated to 105 °C for 30 days in an oven. The as-synthesized sample was purified through repeated washing with DMF to yield small transparent polyhedral crystals (Fig. S3a), which were stable and insoluble in MeOH and CH_2Cl_2 (Fig. S4a). Yield: 41% (based on the crystals dried in air). Anal. calcd. for $C_{42}H_{30}N_2O_{28}Yb_5$: C 26.89, H 1.61, N 1.49%. Found: C 25.75, H 1.63, N 1.09%. IR (KBr, cm^{-1}): 3417(m), 2930(m), 1660(vs), 1615(s), 1570(s), 1385(vs), 1250(m), 1096(m), 1057(w), 1019(w), 945(vw), 918(vw), 783(m), 710(m).

2.3. Preparation of $[Yb_5(\mu_3\text{-}OH)_6(DDIA)_2(H_2O)_6](NO_3)\cdot(solv)_x$ (Yb-DDIA)

The synthesis process of **Yb-DDIA** was similar to that of **Yb-DDPY** except H_4DDIA (5 mg, 0.01 mmol) instead of H_4DDPY. The obtained transparent polyhedral crystals (Fig. S3b) were stable and insoluble in MeOH and CH_2Cl_2 (Fig. S4b). Yield: 30% (based on the crystals dried in air). Anal. calcd. for $C_{44}H_{30}N_2O_{32}Yb_5$: C 26.91, H 1.54, N 1.43%. Found: C 25.36, H 1.39, N 1.08%. IR (KBr, cm^{-1}): 3424(m), 2936(m), 1722(w), 1660(s), 1578(vs), 1385(s), 1249(m), 1102(m), 1026(m), 916(w), 945(vw), 782(m), 748(w), 710(m).

2.4. X-ray crystallography

Crystallographic data of **Yb-DDPY** and **Yb-DDIA** were collected at 100 K with an Apex II diffractometer with Mo-Kα radiation (λ = 0.71073 Å) and a SuperNova diffractometer with Cu-Kα radiation (λ = 1.5418 Å), respectively. The structures were solved by direct methods and refined on F^2 by full-matrix least squares using SHELXTL [15]. The contribution of heavily disordered solvent molecules was treated as diffuse using the SQUEEZE routine of PLATON [16] and refined further using the data generated. The contents of guest molecules are not represented in the unit cell contents for the crystal data. Crystallographic data and experimental details for structural analyses are summarized in Table S1. The CCDC reference numbers 1486519 and 1486520 for **Yb-DDPY** and **Yb-DDIA**.

2.5. Catalytic cycloaddition of CO_2 with epoxides

A 20 mL stainless steel autoclave was charged under a protective atmosphere with catalyst (0.01 mmol, corresponding to 0.05 mmol Yb), TBAB (0.1 mmol) and epoxide (20 mmol) at 25 °C. CO_2 was added until the internal pressure in the system reached 1.0 MPa at 25 °C. The solution was mechanically stirred at 600 rpm. The temperature of the reactor was then raised to 60 °C. After 12 h, the reactor was cooling to room temperature. The catalytic reactions at room temperature and atmospheric pressure were carried out in a 10 mL Schlenk tube, which was charged with catalyst (0.02 mmol, corresponding to 0.1 mmol Yb), TBAB (1.7 mmol) and epoxide (28.6 mmol) then the mixture stirring under 1 atm CO_2 atmosphere for 48 h at room temperature. After catalytic reactions, the catalysts were separated by filtration, and the samples of the reaction mixture were analyzed by GC to determine the conversions. The catalysts were washed abundantly with MeOH and CH_2Cl_2, placed in a vial and soaked in MeOH for at least 6 h and subsequently dried under vacuum at room temperature.

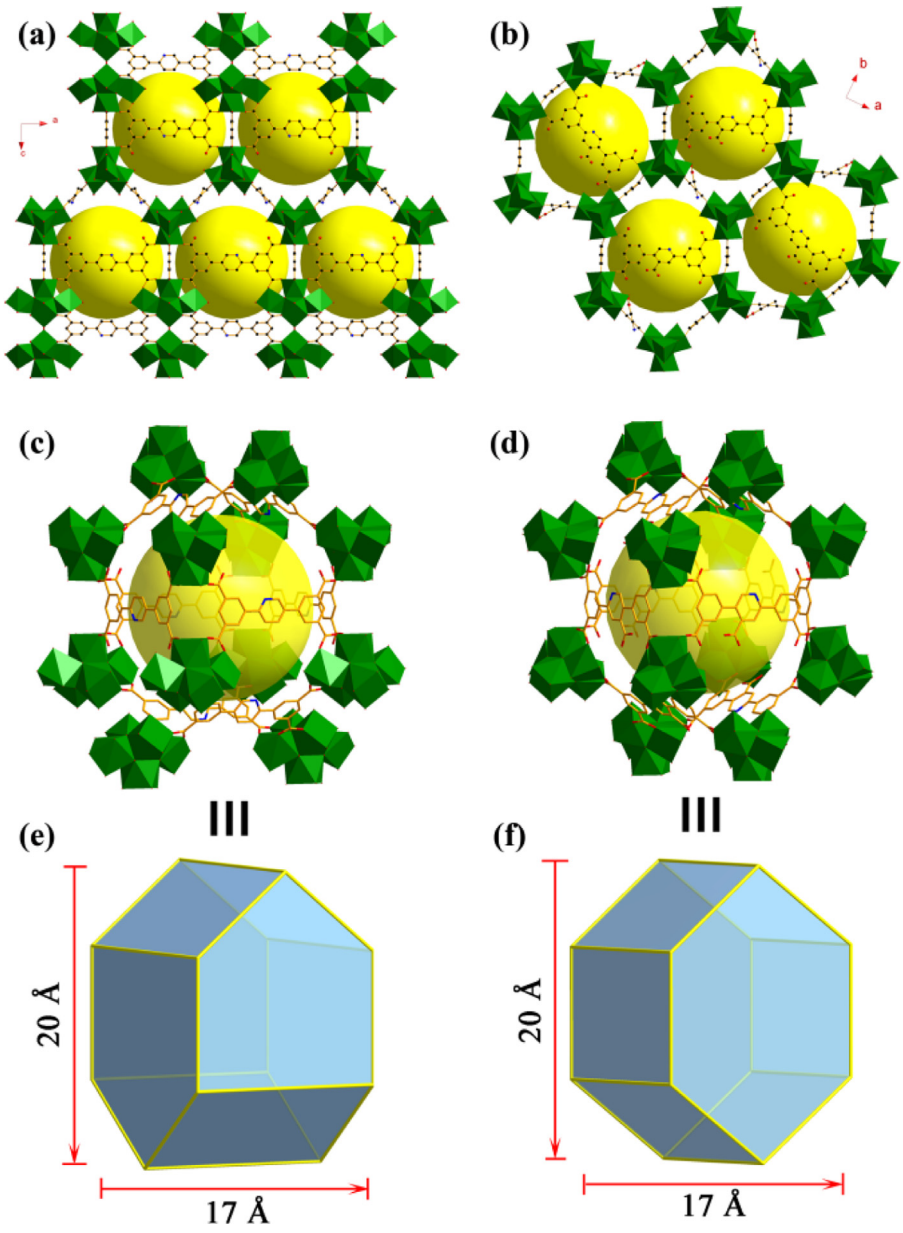

Fig. 2. Views of the networks of Yb-DDPY (a) and Yb-DDIA (b). Polyhedral $M_{12}L_8$-cage in Yb-DDPY (c) and Yb-DDIA (d) and simplification (e-f) of the cages.

3. Results and discussion

3.1. Crystal structure

Single crystal X-ray structural analysis reveals that **Yb-DDPY** crystallizes in the tetragonal space group $I4_1/amd$ and contains pentanuclear Yb(III) cluster secondary building units (SBUs), $[Yb_5(\mu_3\text{-}OH)_6]^{9+}$ (Fig. 1a), showing uncommon trigonal bipyramidal geometry and its triangular faces are capped by six μ_3-OH groups, in which the eight-coordinate Yb1 and Yb3 reside in the equatorial plane and two seven-coordinate Yb2 occupy the apical positions. Each Yb1 and Yb3 with a square-antiprismatic geometry is coordinated by eight oxygen atoms from four μ_3-OH groups, two carboxylate oxygen atoms and two aqua ligands (Yb1)/four carboxylate oxygen atoms (Yb3). Yb2 adopts a mono-capped octahedral coordination geometry defined by seven oxygen atoms from three μ_3-OH groups, three carboxylate oxygen atoms and one aqua ligand (Fig. 1b). All of the trigonal bipyramid vertexes are linked by the coordinated carboxylates to afford $[Yb_5(\mu_3\text{-}OH)_6(O_2C\text{-})_8]$ clusters, presenting a quasiregular double cap triangular prismatic configuration considering only carbon atoms on the carboxylates (Fig. 1c).

The 8-connected $[Yb_5(\mu_3\text{-}OH)_6(O_2C\text{-})_8]$ clusters are connected by DDPY ligands to form a three-dimensional framework (Fig. 2a) with uniform $M_{12}L_8$-cages (Fig. 2c and e). So far, several kinds of cages built from metal ions/clusters (M) and organic linkers (L) have been reported and display various polyhedral configurations, such as tetrahedral M_4L_4 [17] and M_4L_6 [18], octahedral M_6L_4 and M_6L_8 [18], triangular antiprismatic M_6L_{12} [19], cubic M_8L_6 [17] and M_8L_{12} [3], cuboctahedral $M_{12}L_{24}$, rhombicuboctahedral $M_{24}L_{48}$ [18], $M_{12}L_6$ [19], *etc.* The unprecedented $M_{12}L_8$-cage exhibits an interesting polyhedral configuration, which is encircled by 12 Yb_5 clusters occupying every vertex and 8 DDPY ligands embracing every face, with the individual cavity size of *ca.* 20 Å × 17 Å. PLATON analysis [20] revealed that the 3D framework of **Yb-DDPY** was composed of voids of 13951.3 $Å^3$, which represent 59.8% per unit cell volume. The sizes of window apertures of the $M_{12}L_8$-cages were estimated to be *ca.* 8.2 × 10.0 $Å^2$ to 5.5 × 6.7 $Å^2$, considering van der

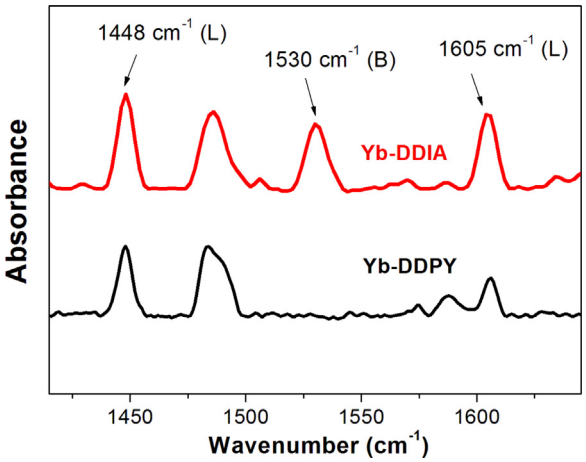

Fig. 3. Py-IR spectra of Yb-DDPY and Yb-DDIA at room temperature.

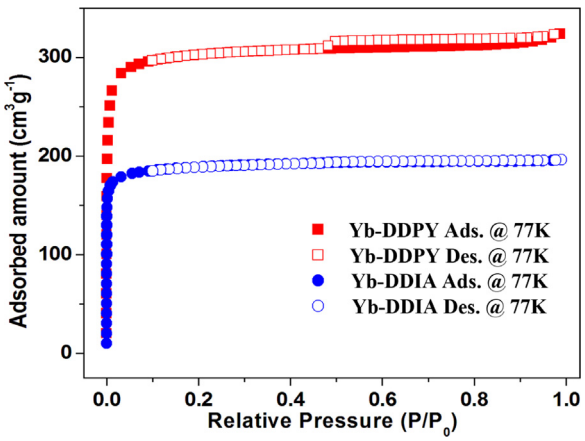

Fig. 4. N_2 adsorption/desorption isotherms of Yb-DDPY and Yb-DDIA at 77 K.

Waals radii (Fig. S11a). After topological simplification, **Yb-DDPY** presents an unprecedented 4,4,8-connected topology (Fig. S12a).

The free carboxyl groups dangled in the pores of the frameworks can act as polar functional sites enhancing the CO_2 adsorption capacity [21–23] and separation of chemical substances [19,24,25], which also can catalyze some organic reactions as Brønsted acidic sites[26]. To introduce carboxyl groups into the framework, another Yb_5 clusters-based MOF (**Yb-DDIA)** was constructed by pyridyl carboxylic acid-supported ligand (H_4DDIA) as linker, which displays a distinguishing structure from **Yb-DDPY**. **Yb-DDIA** crystallizes in the orthorhombic space group *Pbam* and its 8-connected $[Yb_5(\mu_3\text{-}OH)_6]^{9+}$ SBU exhibits a different connection behavior from the one in **Yb-DDPY**. The steric hindrance of the free –COOH group on DDIA makes two monodentate linkers coordinate to two individual Yb atoms rather than one with an included angle of 138.5° (85.9° for **Yb-DDPY**) (Fig. 1c and e). Thus the extension direction of nodes change and another new framework with different topology is generated. The $M_{12}L_8$-cages in **Yb-DDIA** are uniform hexagonal prisms with individual cavity size of *ca.* 20 Å × 17 Å (Fig. 2d and f). PLATON analysis revealed that the 3D framework of **Yb-DDIA** was composed of voids of 11568.4 Å^3, which represent 54.3% per unit cell volume. The openings of the cage, *ca.* 8.3 × 9.8 Å^2 to 6.7 × 7.9 Å^2, are slightly narrow than those in **Yb-DDPY** (Fig. S11b), owing to the free –COOH groups of DDIA ligands. The framework of **Yb-DDIA** can be simplified to a 4,4,4,8-connected net (Fig. S12b).

3.2. Lewis and Brønsted acidity characterization

Yb-DDPY and **Yb-DDIA** are presumably excellent Lewis acidic catalysts owing to the high concentration of the Lewis acidic Yb_5 clusters in their structures, and the free –COOH groups in **Yb-DDIA** are Brønsted acidic sites. In order to evaluate the Lewis and Brønsted acidic sites on the two frameworks, pyridine adsorption fourier-transform infrared (Py-IR) spectroscopy was performed at room temperature. According to the literatures [27], pyridine is a common IR probe for testing acidic sites in solid acid catalysts. The peaks appear in the region between 1700 and 1400 cm^{-1} indicate the ring vibrations of pyridine, which shift depending on whether pyridine is coordinated to a Lewis acidic site or is protonated by a Brønsted acidic site. As shown in Fig. 3, both the peaks at *ca.* 1448 and 1605 cm^{-1} are all in close agreement with the existence of Lewis acidic sites in **Yb-DDPY** and **Yb-DDIA** [28]. Evidence for the Brønsted acidity of **Yb-DDIA** are indicated by the peak at *ca.* 1530 cm^{-1} typical for pyridinium ions bonded to Brønsted acidic sites. The ratios of Lewis to Brønsted acidic sites in **Yb-DDIA** have been estimated by integrating the peaks at 1448 and 1530 cm^{-1}, and the results were summarized in Table S2 (the resulting L:B ratio of 1.41 for **Yb-DDIA**). It's worth mentioning that the Py-IR experiments were carried out at room temperature, and the coordinated water molecules on the Yb(III) centers can not be removed under such conditions, indicating that the seven- or eight-coordinate Yb(III) centers can act as accessible Lewis acidic sites in these materials.

3.3. Gas sorption

Both of the **Yb-DDPY** and **Yb-DDIA** display a fully reversible Type-I isotherm through the investigation of N_2 adsorption at 77 K (Fig. 4), confirming their microporosity. The Brunauer-Emmett-Teller (BET) surface areas of **Yb-DDPY** and **Yb-DDIA** are estimated to be 1226 m^2 g^{-1} (theoretical value of 1451 m^2 g^{-1}) and 759 m^2 g^{-1} (theoretical values of 1236 m^2 g^{-1}), respectively. The latter is smaller than the former due to the occupation of the pores by the free carboxyl groups. The experimental pore volumes of **Yb-DDPY** and **Yb-DDIA** are 0.49 and 0.30 cm^3 g^{-1}, respectively, which lower than the theoretical values (0.57 and 0.49 cm^3 g^{-1}).

When the pressure approaches 760 Torr, the CO_2 uptake of **Yb-DDPY** reaches 247. 67 cm^3 g^{-1} at 195 K and 76.07 cm^3 g^{-1} at 273 K (Fig. 5a), which is higher than reported highly porous MOFs possessing multinuclear metal cluster moieties and cage structure at 273 K, such as PCN-56 (*ca.* 55 cm^3 g^{-1}), PCN-57 (*ca.* 50 cm^3 g^{-1}) [29] and Y-ftw-MOF-2 (*ca.* 56 cm^3 g^{-1}) [30]. **Yb-DDIA** shows a lower CO_2-uptake value of 176.7 cm^3 g^{-1} at 195 K and 58.06 cm^3 g^{-1} at 273 K (Fig. 6a) owing to its smaller pore volume. The isosteric heat of adsorption (Q_{st}) of **Yb-DDPY** and **Yb-DDIA** were calculated based on the CO_2 adsorption isotherms at 195 K, 273 K and 298 K using the Clausius–Clapeyron equation [31], revealing that Q_{st} of **Yb-DDPY** and **Yb-DDIA** at zero surface coverage are 28.37 kJ mol^{-1} and 30.87 kJ mol^{-1}, respectively (Figs. 5b and 6b). The Q_{st} for CO_2 shows similar behavior for **Yb-DDPY** and **Yb-DDIA**, which are progressively slightly decreasing as the CO_2 loading increases, indicating that the effect of porous filling plays key roles over the full range of gas loading [32]. The higher Q_{st} of **Yb-DDIA** is mainly related to the existence of polar free –COOH groups exposed on the pores, which cooperate with the basic pyridine groups on the linkers to facilitate the adsorption of CO_2 [23].

3.4. Cycloaddition of CO_2 and epoxides

Transformation of CO_2 to cyclic carbonates has gained a great deal of attentions in recent years [33–35], and the main reasons can be summarized as follows: (1) CO_2 is one of the major greenhouse gases blamed for the climate change and global warming

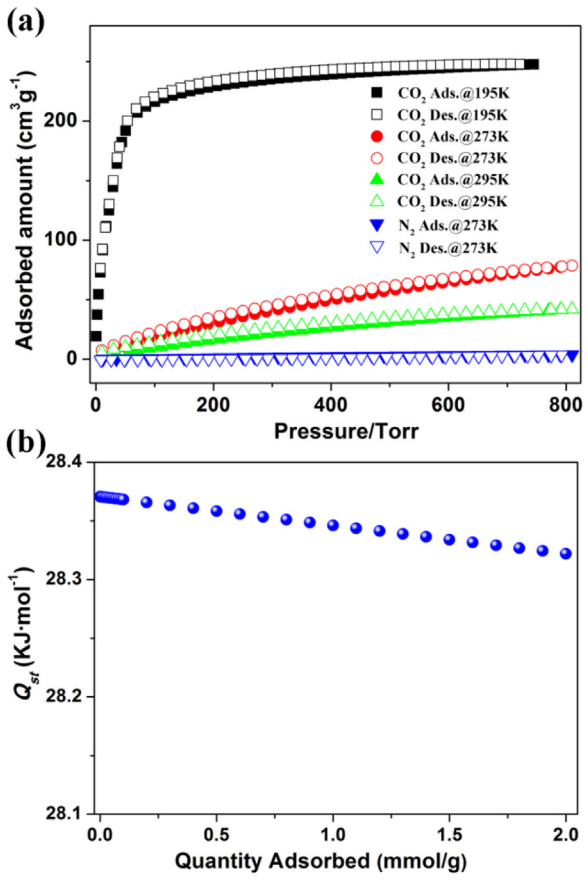

Fig. 5. (a) The adsorption/desorption isotherms of CO_2 (195 K, 273 K and 295 K) and N_2 (273 K) for Yb-DDPY. (b) The isosteric heat of CO_2 adsorption (Q_{st}) of Yb-DDPY calculated from the adsorption isotherms at 195 K, 273 K and 295 K.

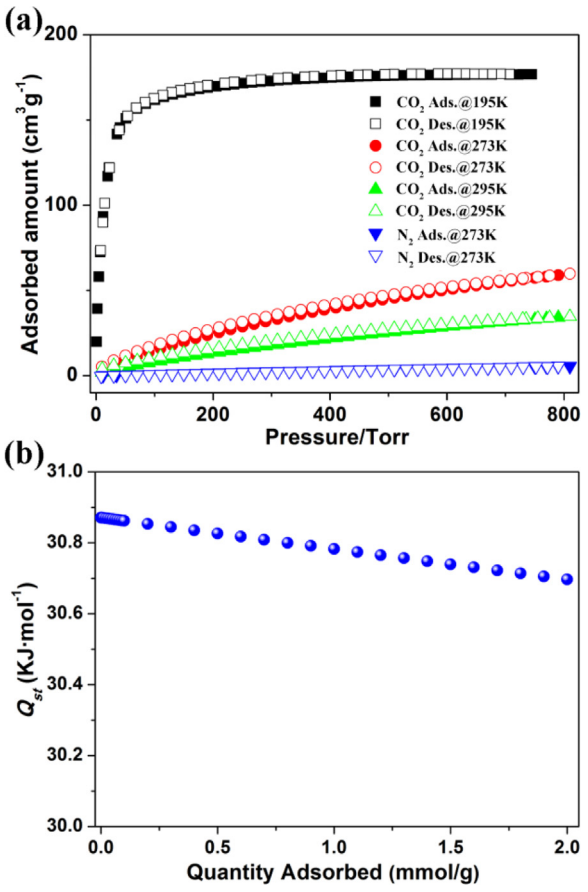

Fig. 6. (a) The adsorption/desorption isotherms of CO_2 (195 K, 273 K and 295 K) and N_2 (273 K) for Yb-DDIA. (b) The isosteric heat of CO_2 adsorption (Q_{st}) of Yb-DDIA calculated from the adsorption isotherms at 195 K, 273 K and 295 K.

[36], so the chemical CO_2 fixation is a challenging and important synthetic goal. (2) In terms of its nontoxicity, easy availability and renewability, CO_2 can be offered as a useful industrial raw material in synthetic chemistry [37–39]. (3) Cyclic carbonates are valuable chemical products owing to their applications as raw materials for engineering plastics and as intermediates in the manufacture of fine chemicals [40,41]. The cycloaddition reaction between CO_2 and epoxides is one of the most powerful and attractive strategies for the CO_2 chemical conversion [42]. The ability of capture CO_2 and the higher accessibility of the Lewis acidic sites in the frameworks, which are deemed necessary for epoxide activation as a first reaction step [43–45], prompt we investigate the catalytic abilities of **Yb-DDPY** and **Yb-DDIA** as heterogeneous catalysts in the cycloaddition reaction of CO_2 with epoxide substrates.

In a typical experiment, the reaction was processed in an autoclave reactor using the propylene oxide (PO, 20 mmol) with CO_2 purged to 1.0 MPa under a solvent-free environment at 60 °C in the presence of 0.1 mmol TBAB (tetrabutylammonium bromide) as co-catalyst [46,47]. The conversions of PO have reached 85% (**Yb-DDPY**) and 93% (**Yb-DDIA**) after 12 h (Table 1, entries 5 and 14). Comparably, as a heterogeneous catalyst, Yb_2O_3 did not display significantly catalytic activity under the same conditions, which provides less accessible Lewis acidic sites since their aggregation behavior in the reaction system (Table 1, entry 1). Under the same conditions, the independent MOFs or TBAB also demonstrate lower catalytic activity for the cycloaddition of PO and CO_2 (Table 1, entries 2–4), and the TON values per mol of Yb (112 for **Yb-DDPY** and 136 for **Yb-DDIA**) are higher than the one per mol of TBAB (60), indicating that the MOFs play a predominant role in the reactions.

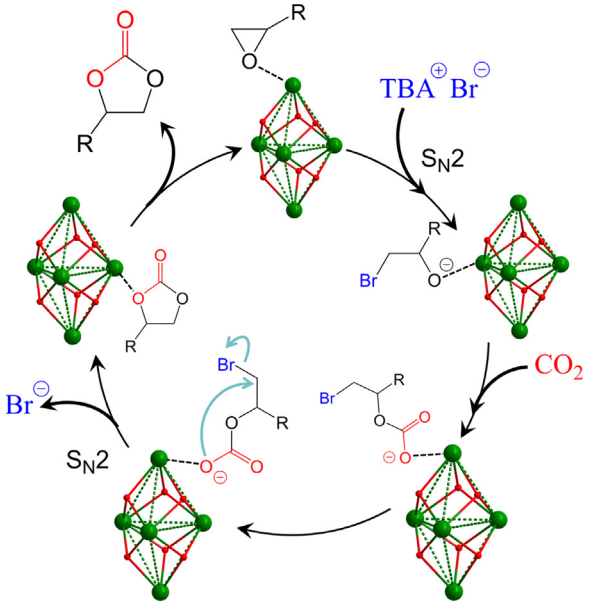

Fig. 7. The proposed mechanism for the cycloaddition reactions catalyzed by Yb-DDPY and Yb-DDIA.

Rare-earth cluster-based MOFs as catalysts for cycloaddition of CO_2 with epoxides have been rarely reported. Eddaoudi and co-workers [48] reported a nonanuclear Y cluster-based MOF, gea-MOF-1, and studied its performance in catalyzing cycloaddition

Table 1
Cycloaddition of CO_2 with various epoxides catalyzed by various catalysts.

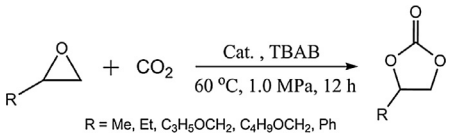

Entry	R	Catalyst	Conversion[a] (%)	TON[b]
1[c]	Me	Yb_2O_3, TBAB	33	132
2	Me	TBAB	30	60
3	Me	Yb-DDPY	28	112
4	Me	Yb-DDIA	34	136
5	Me	Yb-DDPY, TBAB	85	340
6[d]	Me	Yb-DDPY, TBAB	83	332
7[d]	Me	Yb-DDPY, TBAB	82	328
8[d]	Me	Yb-DDPY, TBAB	80	320
9[d]	Me	Yb-DDPY, TBAB	78	312
10	Et	Yb-DDPY, TBAB	74	296
11	$C_3H_5OCH_2$	Yb-DDPY, TBAB	67	268
12	$C_4H_9OCH_2$	Yb-DDPY, TBAB	64	256
13	Ph	Yb-DDPY, TBAB	52	208
14	Me	Yb-DDIA, TBAB	93	372
15[d]	Me	Yb-DDIA, TBAB	92	368
16[d]	Me	Yb-DDIA, TBAB	90	360
17[d]	Me	Yb-DDIA, TBAB	90	360
18[d]	Me	Yb-DDIA, TBAB	89	356
19	Et	Yb-DDIA, TBAB	86	344
20	$C_3H_5OCH_2$	Yb-DDIA, TBAB	83	332
21	$C_4H_9OCH_2$	Yb-DDIA, TBAB	89	356
22	Ph	Yb-DDIA, TBAB	60	240
23[e]	Me	MOF-5, TBAB	97.6	72
24[f]	$C_3H_5OCH_2$	CHB(M), TBAB	89.2	28
25[g]	Ph	1·Gd, TBAB	70	9

Reaction conditions: epoxides (20 mmol), catalyst (0.01 mmol, corresponding to 0.05 mmol Yb, 0.25 mol%), TBAB (0.1 mmol, 0.5 mol%) under CO_2 (1.0 MPa), 60 °C and 12 h.
[a] The conversions were determined by GC.
[b] Moles of epoxides consumed/moles of Yb.
[c] Yb_2O_3 (0.025 mmol, corresponding to 0.05 mmol Yb).
[d] With recycled catalysts from the previous entry.
[e] PO (20 mmol), MOF-5 (100 mg, 0.27 mmol Zn), TBAB (2.5 mol%) at 50 °C, 6.0 MPa for 4 h.
[f] Allyl glycidyl ether (18.6 mmol), CHB(M) (1.6 mol%, 0.30 mmol Cu), TBAB (1.6 mol%) at 80 °C, 1.2 MPa for 6 h.
[g] Styrene oxide (1 mmol), 1·Gd (0.032 mmol Gd), TBAB (2.5 mol%) at 60 °C, 0.1 MPa for 12 h.

Table 2
Cycloaddition of CO_2 with epoxides catalyzed by **Yb-DDPY** and **Yb-DDIA** at room temperature and atmospheric pressure.

Entry	Epoxides	Catalyst	Conversion[a] (%)	TON[b]
1		Yb-DDPY, TBAB	75	215
2		Yb-DDIA, TBAB	85	243
3	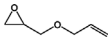	Yb-DDPY, TBAB	66	189
4		Yb-DDIA, TBAB	80	229
5		Yb-DDPY, TBAB	40	114
6		Yb-DDIA, TBAB	48	137

Reaction conditions: epoxides (28.6 mmol), catalyst (0.02 mmol, corresponding to 0.1 mmol Yb), TBAB (1.7 mmol) under CO_2 (1 atm), room temperature and 48 h.
[a] The conversions were determined by GC.
[b] Moles of epoxides consumed/moles of Yb.

reaction of CO_2 with epoxides. The conversion rate of PO catalyzed by gea-MOF-1 reaches 88% at 120 °C under 2.0 MPa CO_2 pressure. Compared with the benchmark MOF catalyst, MOF-5 [49] (Table 1, entry 23), **Yb-DDPY** and **Yb-DDIA** also provide higher TON values under the similar reaction conditions.

The extensive cycloaddition reactions of CO_2 with a variety of epoxides catalyzed by the resultant MOFs were also explored and the results are summarized in Table 1 (entries 10–13, 19–22), which show that the conversions of epoxides display gradual decrement trend with the enlargement of molecular sizes of epoxide substrates. The limited accessible pore diameters of cages allow smaller epoxide substrates to enter into the cavities swiftly then interact with the acidic Yb(III) centers, but the large-sized epoxide substrates exhibit a slower diffusion into the void space within cage, resulting in lower conversions during the same time [46,50,51]. After catalyzing the cycloaddition reaction of CO_2 and butyl glycidyl ether, the catalysts have been washed with MeOH and CH_2Cl_2 to remove the substances on the surface. Then the ^1H NMR of **Yb-DDPY** was carried out and the result confirmed that the reaction product exist inside the catalysts (Fig. S14), indicating that the reactants can enter into the void spaces and the reaction occurred inside the cages of **Yb-DDPY**. Though **Yb-DDIA** possesses smaller cage opening sizes and lower CO_2 adsorption capability, the Brønsted acidic –COOH groups endow **Yb-DDIA** with higher catalytic activity towards the cycloaddition of CO_2 and epoxides than **Yb-DDPY** under the same conditions, which is probably attribute to the synergistic effect of the Brønsted acidic –COOH groups and the Lewis acidic Yb(III) sites [52,53]. For the cycloaddition of CO_2 and allyl gly-

cidyl ether or styrene oxide, other reported catalysts exhibit lower TON values under the similar reaction conditions (Table 1, entries 24 and 25) [47,54].

The cycloaddition of CO_2 and epoxides were also carried out with **Yb-DDPY** and **Yb-DDIA** as catalysts at room temperature and atmospheric pressure. As shown in Table 2, the conversions of smaller PO reach 75% and 85.2% after 48 h, respectively. The conversions of larger allyl glycidyl ether and styrene oxide reach to 66% and 40% (**Yb-DDPY**), 80% and 48% (**Yb-DDIA**), respectively (Table 2, entries 3–6). The results indicated that these Yb_5 cluster-based MOFs also exhibit catalytic activities under mild conditions and **Yb-DDIA** still shows higher catalytic activity due to the synergy of Lewis acidic Yb(III) sites and Brønsted acidic –COOH groups.

Leaching tests have been performed to exclude the contribution of homogeneous Yb-species to the catalytic performance of **Yb-DDPY**/**Yb-DDIA**. The result shows that the transformation of the PO dramatically decreases after removal of catalysts at 4 h (Fig. S15), confirming the heterogeneous nature of the catalysts. The recycling experiments were further carried out for successive runs using recycled **Yb-DDPY**/**Yb-DDIA** and freshly added co-catalyst TBAB. The recycling tests proved that both **Yb-DDPY** and **Yb-DDIA** can serve as excellent recoverable catalysts for the solvent-free cycloaddition reaction of CO_2 with PO in the presence of co-catalyst TBAB, exhibiting nearly equivalent catalytic activity to the previous reactions during 5 cycles of recyclability experiments (Table 1, entries 6–9, 15–18). Moreover, as catalysts, **Yb-DDPY** and **Yb-DDIA** are easily isolated from the reaction suspension by a simple filtration. The PXRD patterns of recycled **Yb-DDPY** and **Yb-DDIA** after 5 cycles were examined, which are almost the same as the fresh ones (Fig. S4), indicating stability of the catalysts.

According to the previous reports [54,55], a tentative mechanism for the cycloaddition of CO_2 and epoxide into cyclic carbonate is proposed to be the Lewis acid based catalysis. As illustrated in Fig. 7, epoxides first bind to the Lewis acidic Yb(III) sites through the oxygen atoms to activate the epoxy ring. Then, TBAB attacks the less-hindered carbon atom of the epoxide using its Br^- as nucleophile to open the epoxy ring. Subsequently, the opened epoxy ring interacts with CO_2 forming an alkylcarbonate anion, which is converted into corresponding cyclic carbonate through the final ring-closing step, and TBAB is recycled simultaneously. To verify the cooperative interactions between the Yb(III) sites and PO, the spectroscopic (IR and ^{1}H NMR) analyses of PO-impregnated **Yb-DDPY** were carried out. IR spectrum of PO-impregnated **Yb-DDPY** revealed two epoxy vibration peaks at 949 and 828 cm^{-1} (Fig. S16). ^{1}H NMR of the PO-impregnated **Yb-DDPY** in DMSO-d_6/DCl/D_2O exhibits the characteristic peaks of PO with significant downfield shifts of free PO (Fig. S17). The obvious shifts of ^{1}H NMR and IR spectra compared with the free PO suggested the adsorption and the activation of the PO in the cages of the MOFs [56]. The higher catalytic activities of **Yb-DDIA** and TBAB system result from the synergistic effect of combining the Brønsted acidic –COOH groups with the Lewis acidic Yb(III) sites [53]. **Yb-DDPY** and **Yb-DDIA** could still lead to low conversions of PO under the same conditions in absence of co-catalyst TBAB (Table 1, entries 3 and 4) due to the weak Lewis base sites (nitrogen atoms on the pyridyl rings) in their frameworks, which could partly replace TBAB to activate CO_2 molecules and subsequently attack the epoxide attached on the Lewis acidic Yb(III) sites [57,58], then facilitates the reaction.

4. Conclusions

In conclusion, two Yb_5 cluster-based MOFs with unique polyhedral cages were constructed, in which the $[Yb_5(\mu_3\text{-}OH)_6]^{9+}$ SBUs present uncommon trigonal bipyramidal geometry. The affinity of CO_2 and existence of Lewis acidic sites make the Yb_5 cluster-based MOFs potential heterogeneous catalysts for chemical conversion of CO_2 with epoxides, which maintain the integrity of the structures and catalytic activity after 5 cycles of reactions, indicating their stability and recyclability. Introducing functional –COOH groups into the framework during the assembly process enhances the catalytic activity of **Yb-DDIA** towards the cycloaddition of CO_2 and epoxide owing to the synergistic effect of the Brønsted acidic –COOH groups and the Lewis acidic Yb(III) sites. The future work is in progress to systematically fabricate the new porous MOFs based on the pentanuclear rare-earth clusters and explore their potential functionality for gas absorption and catalysis.

Acknowledgements

This work was granted financial support from National Key Projects for Fundamental Research and Development of China (2016YFB0600903), National Natural Science Foundation of China (Grant 21671090, 21271096).

Appendix A. Supplementary data

Supplementary data associated with this article can be found, in the online version, at http://dx.doi.org/10.1016/j.apcatb.2017.07.085.

References

[1] H.-C. Zhou, S. Kitagawa, Metal-organic frameworks (MOFs), Chem. Soc. Rev. 43 (2014) 5415–5418.
[2] H. Furukawa, K.E. Cordova, M. O'Keeffe, O.M. Yaghi, The chemistry and applications of metal-organic frameworks, Science 341 (2013) 1230444.
[3] W. Lu, Z. Wei, Z.-Y. Gu, T.-F. Liu, J. Park, J. Park, J. Tian, M. Zhang, Q. Zhang, T. Gentle III, M. Boscha, H.-C. Zhou, Tuning the structure and function of metal-organic frameworks via linker design, Chem. Soc. Rev. 43 (2014) 5561–5593.
[4] B. Li, M. Chrzanowski, Y. Zhang, S. Ma, Applications of metal-organic frameworks featuring multi-functional sites, Coord. Chem. Rev. 307 (2016) 106–129.
[5] T. Islamoglu, S. Goswami, Z. Li, A.J. Howarth, O.K. Farha, J.T. Hupp, Postsynthetic tuning of metal-organic frameworks for targeted applications, Acc. Chem. Res. 50 (2017) 805–813.
[6] G. Xu, Z.-M. Wang, Z. He, Z. Lu, C.-S. Liao, C.-H. Yan, Synthesis and structural characterization of nonanuclear lanthanide complexes, Inorg. Chem. 41 (2002) 6802–6807.
[7] T. Kajiwara, H. Wu, T. Ito, N. Iki, S. Miyano, Octalanthanide wheels supported by *p-tert*-butylsulfonylcalix[4] arene, Angew. Chem. Int. Ed. 43 (2004) 1832–1835.
[8] L.-X. Chang, G. Xiong, L. Wang, P. Cheng, B. Zhao, A 24-Gd nanocapsule with a large magnetocaloric effect, Chem. Commun. 49 (2013) 1055–1057.
[9] G.-M. Wang, J.-H. Li, Z.-X. Li, P. Wang, Y.-X. Wang, J.-H. Lin, Synthesis and structural characterization of a novel two-dimensional 3d-4f heterometallic coordination framework based on pentanuclear lanthanide cluster, Solid State Sci. 14 (2012) 445–450.
[10] P.-F. Shi, Y.-Z. Zheng, X.-Q. Zhao, G. Xiong, B. Zhao, F.-F. Wan, P. Cheng, 3D MOFs containing trigonal bipyramidal Ln_5 clusters as nodes: large magnetocaloric effect and slow magnetic relaxation behavior, Chem. Eur. J. 18 (2012) 15086–15091.
[11] M.T. Gamer, Y. Lan, P.W. Roesky, A.K. Powell, R. Clérac, Pentanuclear dysprosium hydroxy cluster showing single-molecule-magnet behavior, Inorg. Chem. 47 (2008) 6581–6583.
[12] S. Das, A. Dey, S. Kundu, S. Biswas, R.S. Narayanan, S. Titos-Padilla, G. Lorusso, M. Evangelisti, E. Colacio, V. Chandrasekhar, Decanuclear Ln_{10} wheels and vertex-shared spirocyclic Ln_5 cores: synthesis, structure, SMM behavior, and MCE properties, Chem. Eur. J. 21 (2015) 16955–16967.
[13] J.-B. Peng, X.-J. Kong, Y.-P. Ren, L.-S. Long, R.-B. Huang, L.-S. Zheng, Trigonal bipyramidal Dy_5 cluster exhibiting slow magnetic relaxation, Inorg. Chem. 51 (2012) 2186–2190.
[14] S. Feming, C.D. Gutsche, J.M. Harrowfield, M.I. Ogden, B.W. Skelton, D.F. Stewart, A.H. White, Calixarenes as aryloxides: oligonuclear europium(III) derivatives, Dalton Trans. (2003) 3319–3327.
[15] SHELXTL 6.10, Bruker Analytical Instrumentation, Madison, Wisconsin, USA, 2000.
[16] P. van der Sluis, A.L. Spek, BYPASS: an effective method for the refinement of crystal structures containing disordered solvent regions, Acta Crystallogr. A 46 (1990) 194–201.

[17] Y. Bai, Y. Dou, L.-H. Xie, W. Rutledge, J.-R. Li, H.-C. Zhou, Zr-based metal-organic frameworks: design, synthesis, structure, and applications, Chem. Soc. Rev. 45 (2016) 2327–2367.
[18] V. Guillerm, D. Kim, J.F. Eubank, R. Luebke, X. Liu, K. Adil, M.S. Lah, M. Eddaoudi, A supermolecular building approach for the design and construction of metal-organic frameworks, Chem. Soc. Rev. 43 (2014) 6141–6172.
[19] Q. Zhang, J. Yu, J. Cai, R. Song, Y. Cui, Y. Yang, B. Chen, G. Qian, A porous metal-organic framework with -COOH groups for highly efficient pollutant removal, Chem. Commun. 50 (2014) 14455–14458.
[20] A. L. Spek, PLATON, A. M. C. T Utrecht University: Utrecht. The Netherlands, 1998.
[21] S. Biswas, J. Zhang, Z. Li, Y.-Y. Liu, M. Grzywa, L. Sun, D. Volkmer, P.V.D. Voort, Enhanced selectivity of CO_2 over CH_4 in sulphonate-, carboxylate- and iodo-functionalized UiO-66 frameworks, Dalton Trans. 42 (2013) 4730–4737.
[22] J. Li, G.-P. Yang, S.-L. Wei, R.-C. Gao, N.-N. Bai, Y.-Y. Wang, Two microporous metal-organic frameworks with suitable pore size displaying the high CO_2/CH_4 selectivity, Cryst. Growth Des. 15 (2015) 5382–5387.
[23] F. Ragon, B. Campo, Q. Yang, C. Martineau, A.D. Wiersum, A. Lago, V. Guillerm, C. Hemsley, J.F. Eubank, M. Vishnuvarthan, F. Taulelle, P. Horcajada, A. Vimont, P.L. Llewellyn, M. Daturi, S. Devautour-Vinot, G. Maurin, C. Serre, T. Devic, G. Clet, Acid-functionalized UiO-66(Zr) MOFs and their evolution after intra-framework cross-linking: structural features and sorption properties, J. Mater. Chem. A 3 (2015) 3294–3309.
[24] J.B. DeCoste, T.J. Demasky, M.J. Katz, O.K. Farha, J.T. Hupp, A UiO-66 analogue with uncoordinated carboxylic acids for the broad-spectrum removal of toxic chemicals, New J. Chem. 39 (2015) 2396–2399.
[25] S. Demir, N.K. Brune, J.F. Van Humbeck, J.A. Mason, T.V. Plakhova, S. Wang, G. Tian, S.G. Minasian, T. Tyliszczak, T. Yaita, T. Kobayashi, S.N. Kalmykov, H. Shiwaku, D.K. Shuh, J.R. Long, Extraction of lanthanide and actinide ions from aqueous mixtures using a carboxylic acid-functionalized porous aromatic framework, ACS Cent. Sci. 2 (2016) 253–265.
[26] J. Jiang, O.M. Yaghi, Brønsted acidity in metal-organic frameworks, Chem. Rev. 115 (2015) 6966–6997.
[27] M.I. Zaki, M.A. Hasan, F.A. Al-Sagheer, L. Pasupulety, In situ FTIR spectra of pyridine adsorbed on SiO_2-Al_2O_3, TiO_2, ZrO_2 and CeO_2: general considerations for the identification of acid sites on surfaces of finely divided metal oxides, Colloids Surf. A 190 (2001) 261–274.
[28] S.A. Bagshaw, R.P. Cooney, FTIR surface site analysis of pillared clays using pyridine probe species, Chem. Mater. 5 (1993) 1101–1109.
[29] H.-L. Jiang, D. Feng, T.-F. Liu, J.-R. Li, H.-C. Zhou, Pore surface engineering with controlled loadings of functional groups *via* click chemistry in highly stable metal-organic frameworks, J. Am. Chem. Soc. 134 (2012) 14690–14693.
[30] R. Luebke, Y. Belmabkhout, Ł.J. Weseliński, A.J. Cairns, M. Alkordi, G. Norton, Ł. Wojtas, K. Adila, M. Eddaoudi, Versatile rare earth hexanuclear clusters for the design and synthesis of highly-connected ftw-MOFs, Chem. Sci. 6 (2015) 4095–4102.
[31] L. Cepirski, J. Jagiello, Virial-type thermal equation of gas-solid adsorption, Chem. Eng. Sci. 44 (1989) 797–801.
[32] D.-X. Xue, A.J. Cairns, Y. Belmabkhout, L. Wojtas, Y. Liu, M.H. Alkordi, M. Eddaoudi, Tunable rare-earth fcu-MOFs: a platform for systematic enhancement of CO_2 adsorption energetics and uptake, J. Am. Chem. Soc. 135 (2013) 7660–7667.
[33] C. Martín, G. Fiorani, A.W. Kleij, Recent advances in the catalytic preparation of cyclic organic carbonates, ACS Catal. 5 (2015) 1353–1370.
[34] R.R. Kuruppathparambil, T. Jose, R. Babu, G.-Y. Hwang, A.C. Kathalikkattil, D.-W. Kim, D.-W. Park, A room temperature synthesizable and environmental friendly heterogeneous ZIF-67 catalyst for the solvent less and co-catalyst free synthesis of cyclic carbonates, Appl. Catal. B 182 (2016) 562–569.
[35] H. He, J.A. Perman, G. Zhu, S. Ma, Metal-organic frameworks for CO_2 chemical transformations, Small 12 (2016) 6309–6324.
[36] M.H. Beyzavi, R.C. Klet, S. Tussupbayev, J. Borycz, N.A. Vermeulen, C.J. Cramer, J.F. Stoddart, J.T. Hupp, O.K. Farha, A hafnium-based metal-organic framework as an efficient and multifunctional catalyst for facile CO_2 fixation and regioselective and enantioretentive epoxide activation, J. Am. Chem. Soc. 136 (2014) 15861–15864.
[37] S. Liu, F. Chen, S. Li, X. Peng, Y. Xiong, Enhanced photocatalytic conversion of greenhouse gas CO_2 into solar fuels over g-C_3N_4 nanotubes with decorated transparent ZIF-8 nanoclusters, Appl. Catal. B 211 (2017) 1–10.
[38] T. Sakakura, J.C. Choi, H. Yasuda, Transformation of carbon dioxide, Chem. Rev. 107 (2007) 2365–2387.
[39] J. Qin, S. Wang, X. Wang, Visible-light reduction CO_2 with dodecahedral zeolitic imidazolate framework ZIF-67 as an efficient co-catalyst, Appl. Catal. B 209 (2017) 476–482.
[40] S. Fukuoka, M. Kawamura, K. Komiya, M. Tojo, H. Hachiya, K. Hasegawa, M. Aminaka, H. Okamoto, I. Fukawa, S. Konno, A novel non-phosgene polycarbonate production process using by-product CO_2 as starting material, Green Chem. 5 (2003) 497–507.
[41] J.H. Clements, Reactive applications of cyclic alkylene carbonates, Ind. Eng. Chem. Res. 42 (2003) 663–674.
[42] M.H. Beyzavi, C.J. Stephenson, Y. Liu, O. Karagiaridi, J.T. Hupp, O.K. Farha, Metal-organic framework-based catalysts: chemical fixation of CO_2 with epoxides leading to cyclic organic carbonates, Front. Energy Res. 2 (2015) 63.
[43] W.-Y. Gao, H. Wu, K. Leng, Y. Sun, S. Ma, Inserting CO_2 into aryl C-H bonds of metal-organic frameworks: CO_2 utilization for direct heterogeneous C-H activation, Angew. Chem. Int. Ed. 55 (2016) 5472–5476.
[44] R.L. Paddock, Y. Hiyama, J.M. McKay, S.T. Nguyen, Co(III) porphyrin/DMAP: an efficient catalyst system for the synthesis of cyclic carbonates from CO_2 and epoxides, Tetrahedron Lett. 45 (2004) 2023–2026.
[45] A. Decortes, A.M. Castilla, A.W. Kleij, Salen-complex-mediated formation of cyclic carbonates by cycloaddition of CO_2 to epoxides, Angew. Chem. Int. Ed. 49 (2010) 9822–9837.
[46] W.Y. Gao, Y. Chen, Y. Niu, K. Williams, L. Cash, P.J. Perez, L. Wojtas, J. Cai, Y.S. Chen, S. Ma, Crystal engineering of an nbo topology metal-organic framework for chemical fixation of CO_2 under ambient conditions, Angew. Chem. Int. Ed. 53 (2014) 2615–2619.
[47] J. Dong, P. Cui, P.-F. Shi, P. Cheng, B. Zhao, Ultrastrong alkali-resisting lanthanide-zeolites assembled by [Ln_{60}] nanocages, J. Am. Chem. Soc. 137 (2015) 15988–15991.
[48] V. Guillerm, Ł.J. Weseliński, Y. Belmabkhout, A.J. Cairns, V. D'Elia, Ł. Wojtas, K. Adil, M. Eddaoudi, Discovery and introduction of a (3,18)-connected net as an ideal blueprint for the design of metal-organic frameworks, Nat. Chem. 6 (2014) 673–680.
[49] J. Song, Z. Zhang, S. Hu, T. Wu, T. Jiang, B. Han, MOF-5/*n*-Bu_4NBr: an efficient catalyst system for the synthesis of cyclic carbonates from epoxides and CO_2 under mild conditions, Green Chem. 11 (2009) 1031–1036.
[50] A. Dhakshinamoorthy, H. Garcia, Cascade reactions catalyzed by metal organic frameworks, ChemSusChem 7 (2014) 2392–2410.
[51] A. Corma, H. Garcıa, F.X.L.I. Xamena, Engineering metal organic frameworks for heterogeneous catalysis, Chem. Rev. 110 (2010) 4606–4655.
[52] M. Zhu, M.A. Carreon, Porous crystals as active catalysts for the synthesis of cyclic carbonates, J. Appl. Polym. Sci. 131 (2014) 39738.
[53] L. Liu, S.-M. Wang, Z.-B. Han, M. Ding, D.-Q. Yuan, H.-L. Jiang, Exceptionally robust In-based metal-organic framework for highly efficient carbon dioxide capture and conversion, Inorg. Chem. 55 (2016) 3558–3565.
[54] A.C. Kathalikkattil, D.-W. Kim, J. Tharun, H.-G. Soek, R. Roshan, D.-W. Park, Aqueous-microwave synthesized carboxyl functional molecular ribbon coordination framework catalyst for the synthesis of cyclic carbonates from epoxides and CO_2, Green Chem. 16 (2014) 1607–1616.
[55] Z.-R. Jiang, H. Wang, Y. Hu, J. Lu, H.-L. Jiang, Polar group and defect engineering in a metal-organic framework: synergistic promotion of carbon dioxide sorption and conversion, ChemSusChem 8 (2015) 878–885.
[56] Z. Zhou, C. He, J. Xiu, Lu Yang, C. Duan, Metal-organic polymers containing discrete single-walled nanotube as a heterogeneous catalyst for the cycloaddition of carbon dioxide to epoxides, J. Am. Chem. Soc. 137 (2015) 15066–15069.
[57] X.B. Lu, B. Liang, Y.J. Zhang, Y.Z. Tian, Y.M. Wang, C.X. Bai, H. Wang, R. Zhang, Asymmetric catalysis with CO_2: direct synthesis of optically active propylene carbonate from racemic epoxides, J. Am. Chem. Soc. 126 (2004) 3732–3733.
[58] J. Kim, S.-N. Kim, H.-G. Jang, G. Seo, W.-S. Ahn, CO_2 cycloaddition of styrene oxide over MOF catalysts, Appl. Catal. A 453 (2013) 175–180.